Resistor Network Analogy of Non-obtuse Finite Element Model for Electrical Impedance Tomography

M. Komarudin
Electrical Engineering Department, Lampung University
komar@unila.ac.id
STMIK Teknokrat Bandar Lampung

Abstract--*This paper introduces resistor network analogy of Finite Element Modelling (FEM). The nonlinear iterative algorithms for image reconstruction in Electrical Impedance Tomography (EIT) involve computation with large matrices resulting from FEM. Consequently, it is difficult to realise real-time solutions. By recognising that a non-obtuse finite element model can be considered to be equivalent to a resistor network, the proposed technique employs matrices of resistors that emulate the elements of a conventional mesh. Software simulations explore the accuracy in the forward solution for Electrical Impedance Tomography application. Results of simulation suggest that forward problem can be solved efficiently using iterative methods with reduced tolerance*

Keywords: *Resistor Networks, Electrical Impedance Tomography, Finite Element Modelling*

A. Introduction

Many problems in engineering and science are characterised by partial differential equations (PDEs). Solutions to these equations can be solved either analytically or numerically. However, in practical models, analytical solutions are very difficult to obtain and numerical approximations are usually used to obtain solutions by means of computers. The finite element method (FEM) is a numerical approximation that is feasible for solving PDEs with complex geometries and non-trivial boundary [1]. In order to approximate solutions to complex engineering problems, FEM subdivides the problem into smaller more manageable elements, which are finite. In this way, partial differential equations that describe the physical laws of the problems are approximated by a set of linear equations, which can easily be solved using the standard techniques of matrix algebra.

In Electrical Impedance Tomography (EIT), the inverse problem is to reconstruct images that estimate the electrical conductivity and/or permittivity distributions in the interior of a body from measurements on its boundary. Usually an array of electrodes is mounted on the body, currents are injected to the electrodes and voltage measurements are collected from the electrodes. FEM is employed as the forward problem solver that determines the calculated boundary data from conductivity distribution by using Laplace's equation. In order to solve the inverse problem, the solution of the forward problem is used as an integral part of the inversion algorithm in which the calculated response from the forward problem is compared to the measured response or observed data. Using nonlinear iterative algorithms, the corresponding calculated boundary that fits best to the observed data is sought iteratively to predict the conductivity distribution.

The nonlinear iterative algorithms for image reconstruction in EIT involve computation with large matrices. Consequently, the computational demands of solving the forward problem are significant and it is difficult to realise real-time solutions to satisfy the demands of many industrial applications, and iterative

Naskah ini diterima pada tangal 28 Mei 2007, direvisi pada tanggal 3 Juli 2007 dan disetujui untuk diterbitkan pada tanggal 1 Agusus 2007

image reconstruction is typically only feasible for off-line processing. In order to improve processing times, it is desirable to exploit the parallelism that is inherent in hardware solutions. By recognising that a non-obtuse finite element model can be considered to be equivalent to a resistor network [2] it becomes natural to consider the realisation of FEM using networks of programmable components that emulate the elements of a conventional mesh. The idea of using such a resistor network to solve field problems in real time is not new [3] but it has become a practical reality with the availability of sub-micron VLSI technology.

Most EIT systems solve the forward problem using software running on conventional digital computers. Double precision accuracy is usually used in the computation in order to minimise the truncation error. However for digital VLSI, double precision arithmetic is very costly in terms of silicon area and consequently a high degree of parallelism is not readily achievable. An alternative is to consider analogue computation, which is unable to offer "double precision" accuracy due to the inherent effects of noise. Consequently, it is necessary to investigate the effect of reducing the accuracy of computation. This paper describes the simulation of resistor networks to determine the lower bounds on accuracy that may be appropriate for providing solutions for EIT.

B. Physical models in EIT

In order to reconstruct an image of a conductivity distribution inside the body, the first step is to construct a physical model in which a set of equations is derived to relate the injected currents and measured voltages on the boundary with a conductivity distribution inside the body. Figure 1 (a) shows a tank having 16 electrodes around the boundary with conductive and non-conductive materials inside the tank. Physical models in EIT are constructed from Maxwell's equations of electromagnetism [4]. The equations of physical models can be separated into two parts, the equation inside the body and the equation on the boundary.

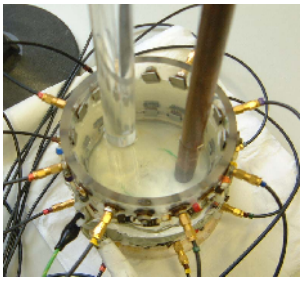

(a)

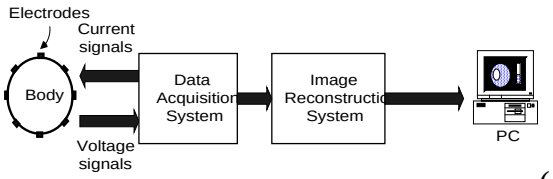

(

b)

Figure1: (a) A tank with 16 electrodes imaging perspex and a copper rod in tap water and (b) the block diagram of a typical EIT system

The governing equation inside the body that describes the potential distribution everywhere within an inhomogeneous and isotropic region is

$$\nabla \cdot (\sigma \nabla \phi) = 0 \quad (1)$$

The boundary conditions refer to electrode models that arise from the current injection and voltage measurement through the electrodes. The model should reflect the exact boundary location, geometry and contact impedance of the electrode pair [5]. The realistic model is the complete electrode model that takes into account both the shunting effect of the electrodes and contact impedances between the electrode and the tissue or the saline solution. Somersalo *et al* [6] has shown that this model agrees well with physical measurement. The complete electrode model in EIT is shown in Figure 2 [7]

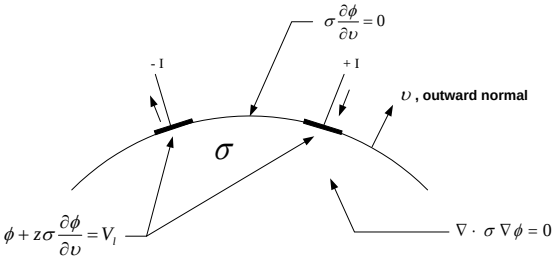

Figure 2: The complete electrode pair model in electrical resistance tomography

where ϕ is the electric scalar potential, σ is conductivity, z is contact impedance, υ is the outward normal vector and V_l is the potential on electrode l. The index l ranges from 1 to L, and L is the number of electrodes. Figure 2 illustrates the complete electrode model that consists of Equation (1) and the boundary conditions. Current on the source electrode is as follows

$$\int \sigma \frac{\partial \phi}{\partial \upsilon} = +I \qquad (2)$$

EIT hardware

The structure of a typical EIT system consists of three main parts: electrodes that are attached on the surface of the body, a data acquisition system that is used to inject current(s) and to measure the voltage signals and a computer to process the measured data that are used to reconstruct the image. Figure 1 (b) depicts the block diagram of an EIT system. A set of linearly independent measurements has to be collected by probing via boundary electrodes in order to obtain the maximum amount of information about the conductivity distribution inside the body. In the adjacent strategy, current is injected through two adjacent electrodes and the voltage measured between pairs of neighbouring electrodes. The procedure is repeated for all electrodes in order to collect all independent measurements. With this strategy, a 16 electrode arrangement has 120 independent voltage measurements since the reciprocity theorem states that an identical value of conductivity will be obtained by reversing the injected current and voltage measurement electrodes [8]. However, voltage measurement at current-injecting electrodes is avoided due to the contact impedance problem. Hence, only 104 independent measurements are collected from 16 electrodes or in general, there are *N(N-3)/2* independent measurements *M* for *N* number of electrodes.

C. Finite Element Modelling as the Forward Problem Solver in EIT

To solve Equation (1) in domain Ω using FEM, the continuous function $\phi(x,y)$ of the problem is turned into piecewise approximation $\Phi(x,y)$ by discretising the solution domain into a finite number of elements. The accuracy of the approximation is strongly dependent on the quality of discretisation. A large number of small-sized elements can approximate the continuous function more accurately than few large elements. In each element, the conductivity is assumed to be homogeneous and isotropic. The popular fundamental element shapes in 2D are triangles. In this paper, triangles are used as elements and the vertices of triangles are called the nodes. Figure 3 (b) shows triangular elements used to discretise a circular domain in Figure 3 (a).

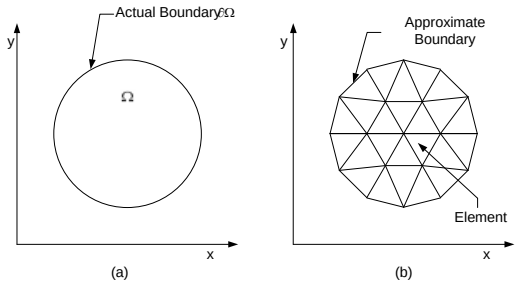

Figure 3: (a) Solution domain Ω, (b) discretisation solution domain using triangular elements.

The approximated solution with N elements can be expressed as follows,

$$\Phi(x,y) = \sum_{e=1}^{N} \Phi^e(x,y) \quad (3)$$

where the superscript e identifies the element, and $\Phi^e(x,y)$ is an approximation of the element such that,

$$\Phi^i(x,y) = 0 \text{ for i = 1 to N, and i} \neq \text{e} \quad (4)$$

Figure 4 (a) shows a single element in a 2D domain with conductivity σ. For every single element in Figure 3 (b), the potentials are adequately approximated by a linear interpolation function based on Figure 4 (a),

$$\Phi = a + bx + cy \quad (5)$$

where a, b and c are coefficients that can be obtained by solving three independent simultaneous equations in (5)

$$\begin{aligned} \Phi_1 &= a + bx_1 + cy_1 \\ \Phi_2 &= a + bx_2 + cy_2 \\ \Phi_3 &= a + bx_3 + cy_3 \end{aligned} \quad (6)$$

where Φ_1, Φ_2 and Φ_3 are potentials at the three vertices. The energy associated with a single triangular element is

$$W^e = \frac{1}{2}\sum_{i=1}^{3}\sum_{j=1}^{3} \Phi_i \int_S \sigma \, \nabla\alpha_i \cdot \nabla\alpha_j \, ds \, \Phi_j \quad (7)$$

The integral term defines the i, j-th matrix element

$$\mathbf{Y}^e = \begin{bmatrix} Y_{11} & Y_{12} & Y_{13} \\ Y_{21} & Y_{22} & Y_{23} \\ Y_{31} & Y_{32} & Y_{33} \end{bmatrix} \quad (8)$$

where

$$\begin{aligned} Y_{ij}^e &= \sigma \iint \nabla\alpha_i \cdot \nabla\alpha_j \, dS \\ &= \frac{\sigma}{4A}\left(b_i b_j + c_i c_j\right) \end{aligned} \quad (9)$$

A is the area of triangle and

$$\begin{aligned} b_1 &= y_2 - y_3, \quad b_2 = y_3 - y_1, \quad b_3 = y_1 - y_2 \\ c_1 &= x_3 - x_2, \quad c_2 = x_1 - x_3, \quad c_3 = x_2 - x_1 \end{aligned} \quad (10)$$

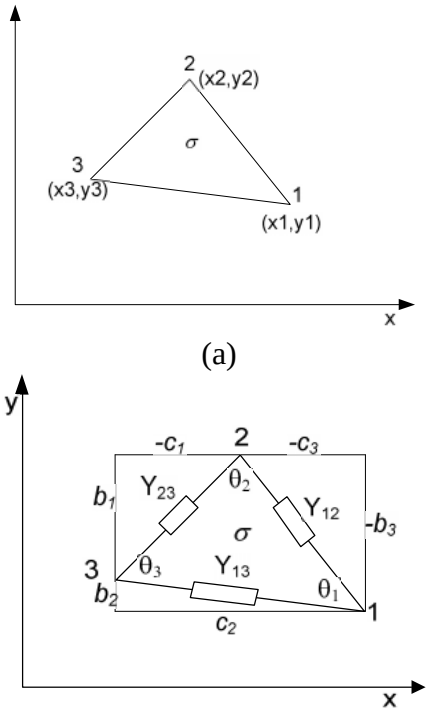

(a)

(b)

Figure 4: (a) A typical triangular element in x-y plane (b) Circuit representation of triangular element where $Y_{ij} > 0$

Resistance Network Analogy

It has been noted since the earliest development of FEM that an equivalent electrical network composed of familiar components such as capacitors, inductors and resistors can represent the triangular mesh. In the case of EIT, the finite element model with linear approximation is equivalent to a resistor network. This representation is only reliable for non-obtuse triangles since the obtuse angles can give negative resistances that are not physically possible. Fortunately, non-obtuse triangles are desirable to construct "well-shaped" elements in FEM [9] since obtuse triangles can affect numerical stability and convergence to undesirable behaviour [10]. The circuit representation for an element in a conductance system

with linear approximation depicted in Figure 4 (a) is shown in Figure 4 (b). $Y_{ij}\left(i, j=1,2,3\right)$ is a conductance between node *i* and node *j* which relates the element geometry to the element conductivity given by

$$Y_{ij} = -\frac{1}{2}\sigma\frac{b_i b_j + c_i c_j}{b_i c_j - c_i b_j} = \frac{1}{2}\sigma\cot\left(\theta_k\right) \quad (11)$$

b_i and c_i are geometric coefficients as given in (10), σ is the element conductivity, and angles θ_k are the non-obtuse corner angles of the element. The admittance matrix for a single disconnected element is defined as

$$\begin{bmatrix} Y_{12}+Y_{13} & -Y_{12} & -Y_{13} \\ -Y_{12} & Y_{12}+Y_{23} & -Y_{23} \\ -Y_{13} & -Y_{23} & Y_{13}+Y_{23} \end{bmatrix} \begin{bmatrix} v_1 \\ v_2 \\ v_3 \end{bmatrix} = \begin{bmatrix} i_1 \\ i_2 \\ i_3 \end{bmatrix} \quad (12)$$

where $i_i = \left(i=1,2,3\right)$ is a prescribed current which flows into ith node and $v_i\left(i=1,2,3\right)$ is a nodal potential on the three vertices of the triangle. The procedure to assemble elements as above can be expressed by modelling each element as a three-resistor network as shown in Figure 5. Using this model, it is well known that the parallel arrangement of conductances can be replaced by a conductance whose value is simply the sum of the individual conductances.

The boundary conditions involve electrode models that arise from current injection and voltage measurement through the electrodes. Using the complete electrode model, Equation is as follows [11],

$$\begin{bmatrix} Y_{con}+Y_Z & Y_V \\ Y_V^T & Y_D \end{bmatrix} \begin{bmatrix} U_{con} \\ V_L \end{bmatrix} = \begin{bmatrix} 0 \\ I^D \end{bmatrix} \quad (13)$$

Components Y_Z, Y_V and Y_D results from the complete electrode model. For the elements with no contact with the electrodes, the corresponding Y_Z entries are zero. In order to preserve the existence and uniqueness of the forward solution the following additional conditions have to be imposed [6]

$$\sum_{l=1}^{L} I_i^D = 0 \quad (14)$$

$$\sum_{l=1}^{L} V_L = 0 \quad (15)$$

where L is the number of electrodes. Equation (14) and (15), corresponding to Kirchoff's laws, state that the net current flowing into a body equals to zero and the sum of the voltage drops in any closed path in a circuit and the electromotive forces in that path is equal to zero.

A resistance network for the complete electrode model can be extracted from Equation (13). Assuming that l elements are located underneath an electrode as

$$\partial\Omega_E = \bigcup_{i=1}^{l} \partial\Omega_{Ei} \quad (16)$$

and substituting the equation beneath electrode in Figure 2 and (6) into (2), the following equation is obtained

$$I_l = \int_{\partial\Omega_E} \frac{1}{z_l}\left(V_l - \phi\right) dl = \sum_{i=1}^{l} \int_{\partial\Omega_{E_i}} \frac{1}{z_l}\left(V_l - \Phi_j \alpha_j\right) dl = \frac{1}{z_l}\left|E_l\right| V_l - \sum_{i=1}^{l} \frac{1}{z_l} \Phi_j \int_{\partial\Omega_{E_i}} \alpha_j dl \quad (17)$$

where $j = 1, \cdots\cdots, 3$ and $\left|E_l\right|$ is the length of the electrode. The components $\frac{\left|E_l\right|}{z_l}$ and $-\sum_{i=1}^{l} \frac{1}{z_l} \int_{\partial\Omega_{E_i}} \alpha_j dl$ in (13) form the compartments Y_D and Y_V of the global conductance matrix in (14) respectively. It can be shown that $\left|E_l\right|$ equals to $\left|\sum_{i=1}^{l} \int_{\partial\Omega_{E_i}} \alpha_j dl\right|$.

For an element underneath the electrode l, let Ω_E be the area of the element and $\partial\Omega_E$ be its boundary that shares the same line with the electrode as shown in Figure 5 (a). Applying the Galerkin method leads to

$$\iint_{\Omega_E} \sigma \nabla \cdot \alpha_i \nabla \Phi = 0 \tag{18}$$

Boundary conditions can be expressed using the left part of (18) by applying the Gauss's theorem

$$\iint_{\Omega_E} \sigma \nabla \cdot \alpha_i \nabla \Phi = \int_{\partial\Omega_E} \sigma \alpha_i \frac{\partial \Phi}{\partial v} \tag{19}$$

Substituting the equation beneath each electrode in Figure 2 and (7) into (19) leads to

$$\iint_{\Omega_E} \sigma \left(\frac{\partial \alpha_i}{\partial x}\frac{\Phi_j \partial \alpha_i}{\partial x} + \frac{\partial \alpha_i}{\partial y}\frac{\Phi_j \partial \alpha_i}{\partial y} \right) dxdy = \int_{\partial\Omega_E} \alpha_i \frac{1}{z_l}\left(V_l - \Phi_j \alpha_j\right) dl \tag{20}$$

where $(i, j) = 1, \cdots\cdots, 3$. Equation (20) can be written as

$$\left[\left(Y_{con} + Y_z\right) - Y_v \right] \begin{bmatrix} \Phi_j \\ V_l \end{bmatrix} = 0 \tag{21}$$

The local matrices $Y_{con}(i, j) \in \sqcup^{3\times3}$, $Y_z(i, j) \in \sqcup^{3\times3}$ and $Y_v(i, j) \in \sqcup^{3}$ that depend on the actual location of the element arise from the various factors of (20) as the following

$$Y_{con}(i, j) = \iint_{\Omega_E} \sigma \left(\frac{\partial \alpha_i}{\partial x}\frac{\Phi_j \partial \alpha_j}{\partial x} + \frac{\partial \alpha_i}{\partial y}\frac{\Phi_j \partial \alpha_j}{\partial y} \right) dx\, dy \tag{22}$$

$$Y_z(i, j) = \int_{\partial\Omega_E} \frac{1}{z_l} \alpha_i \alpha_j dl \tag{23}$$

$$Y_v(i) = \int_{\partial\Omega_E} \frac{1}{z_l} \alpha_i dl \tag{24}$$

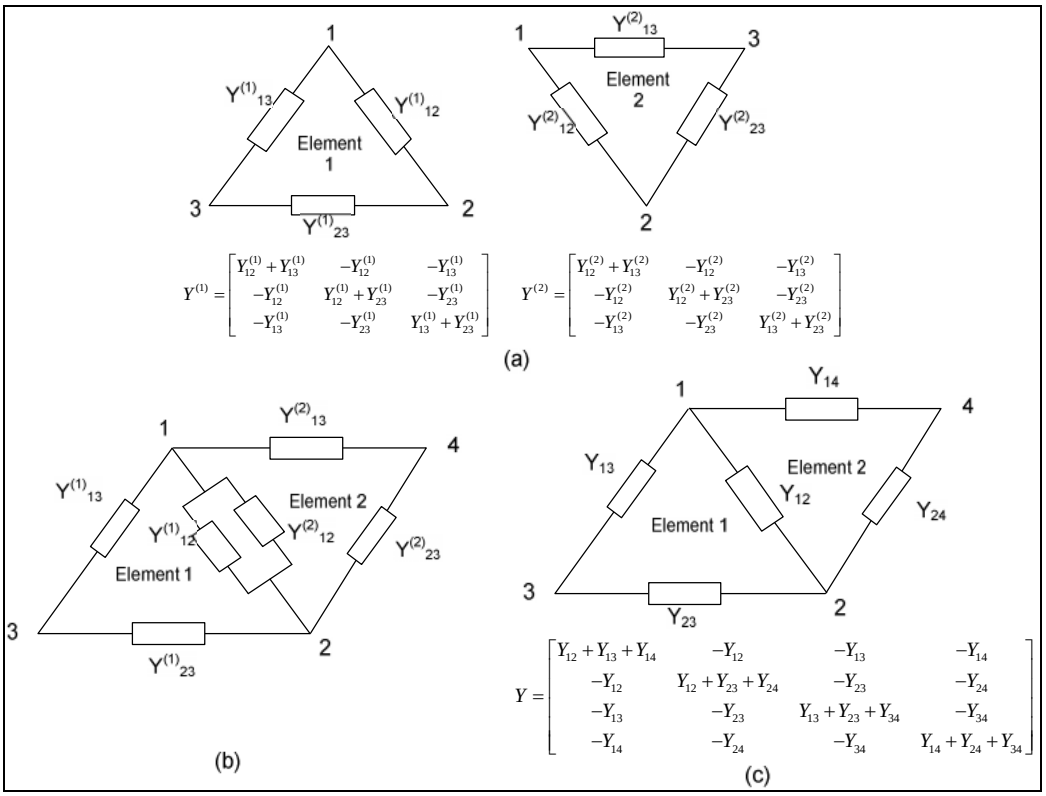

Figure 5 (a) Assembly of two triangular elements (b) conductance arrangement in parallel (c) the overall admittance matrix

$$\begin{bmatrix} \left(-Y_{z12}+Y_{v1}\right) & +Y_{z12} & -Y_{v1} \\ +Y_{z12} & \left(-Y_{z12}+Y_{v2}\right) & -Y_{v2} \\ -Y_{v1} & -Y_{v2} & \left(+Y_{v1}+Y_{v2}\right) \end{bmatrix} \begin{bmatrix} \Phi_1 \\ \Phi_2 \\ V_l \end{bmatrix} = \begin{bmatrix} 0 \\ 0 \\ I_l \end{bmatrix} \quad (25)$$

$$\begin{bmatrix} \left(+Y_{con12}+Y_{con13}\right) & -Y_{con12} & -Y_{con13} \\ -Y_{con12} & \left(+Y_{con12}+Y_{con23}\right) & -Y_{con23} \\ -Y_{con13} & -Y_{con23} & \left(+Y_{con13}+Y_{con23}\right) \end{bmatrix} \begin{bmatrix} \Phi_1 \\ \Phi_2 \\ \Phi_3 \end{bmatrix} = \begin{bmatrix} 0 \\ 0 \\ 0 \end{bmatrix} \quad (26)$$

$$\begin{bmatrix} \left(+Y_{con12}+Y_{con13}-Y_{z12}+Y_{v1}\right) & \left(-Y_{con12}+Y_{z12}\right) & -Y_{con13} & -Y_{v1} \\ \left(-Y_{con12}+Y_{z12}\right) & \left(+Y_{con12}+Y_{con23}-Y_{z12}+Y_{v2}\right) & -Y_{con23} & -Y_{v2} \\ -Y_{con13} & -Y_{con23} & \left(+Y_{con13}+Y_{con23}\right) & 0 \\ -Y_{v1} & -Y_{v2} & 0 & \left(+Y_{v1}+Y_{v2}\right) \end{bmatrix} \cdot \begin{bmatrix} \Phi_1 \\ \Phi_2 \\ \Phi_3 \\ V_l \end{bmatrix} = \begin{bmatrix} 0 \\ 0 \\ 0 \\ I_l \end{bmatrix} \quad (27)$$

Let one element is located underneath of an electrode. Equations (22), (23) and (24), the resistor networks can be written as follows, where Equation (25) and (26) represent the electrode and the element underneath of the electrode respectively. Figure 6(b) shows the resistor networks resulting from those equations. The bottom resistor network represents Y_{con} whereas the top resistor network represents Y_z and Y_v. It can be seen from Equation (26), the non-diagonal component of conductance Y_{z12} in the conductance matrix is positive. Figure 6(b) shows the realised conductance of Y_{z12} resulting from Equation (26). By assembling the top and bottom resistor networks, the resulting matrix as follows, Figure 6(c) shows the resistor network resulting from the assembly process. Although conductance Y_z is negative, the resulting conductance $\left(Y_{con12}-Y_{z12}\right)$ can be positive and this can be achieved by setting Y_{con12} greater than Y_{z12} and the positive conductance can be achieved as follows,

$$\frac{1}{2}\sigma\ Cot\left(\theta_k\right) > \frac{1}{6}\frac{\left|E_l\right|}{z_l} \quad (28)$$

For an electrode with some elements, Equations (17), (22), (23) and (24) are evaluated for each of the elements and are assembled in order to construct the global conductance matrix (13).

D. Results of Simulation

A 16-electrode sensor is assumed into which current is injected on an adjacent pair and on which voltage measurements are made with reference to the centre of the body. 'True' measurements are calculated using the direct method by introducing Gaussian noise of 0.3 x 10^{-4} to the forward solution consisting of 3,136 elements and 1,633 vertices. With this noise level, four significant digit accuracy of 'true' measurements is guaranteed. Using the same mesh, the forward solution is calculated with incomplete Cholesky factorisation for a sequence of tolerances ranging from 10^{-1} to 10^{-12}. To evaluate the quality of boundary measurements, an error is defined as the average of discrepancies between the 'true' measured voltages on the electrodes and the calculated voltages for each tolerance. The error is given by

$$Error = \frac{\sum_{i=1}^{m\times n}\left\|\frac{V_i^{true}-V_i^{fwd}}{V_i^{true}}\right\|}{\left(m\times n\right)}\times 100\% \quad (29)$$

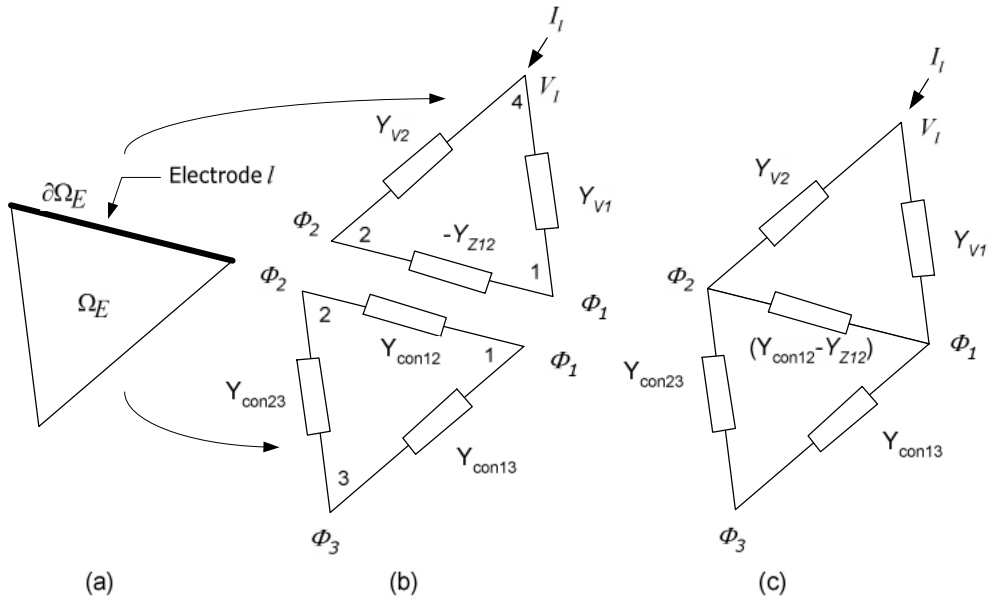

Figure 6: (a) An element underneath the electrode l, (b) the resistance network representations, (c) the sum of resistance network representations

where m is the calculated voltage on the boundary for each n current drive pair. Figure 7 shows the relationship between tolerance of the forward solution and error on the boundary voltage. The graph suggests that the error is fixed at 0.01 % for the tolerance range 4 x 10^{-4} to 2 x 10^{-12} and any refinement performed within this range have no impact on the quality of calculated boundary voltage.

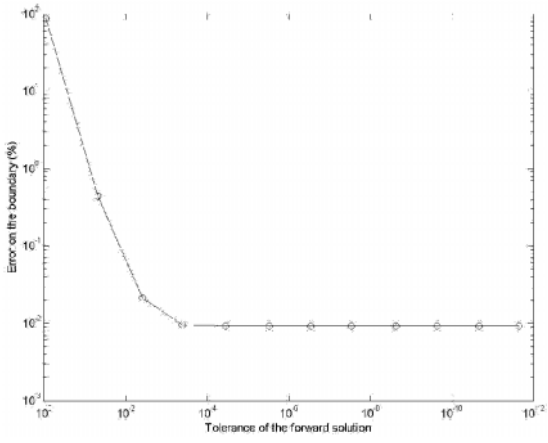

Figure 7: Error of boundary voltages for various tolerances of the forward problem solution

It is interesting to see the graph in Figure 7 as sequences of approximations to the solution, starting from low accuracy (87% error) at tolerance 9 x 10^{-1} and halting the sequence when accuracy is compatible with the accuracy of the measurements. This view suggests that the forward problem can be solved efficiently using iterative methods with reduced tolerance.

Iterative methods produce a sequence of approximations to the solution of a linear system of equations by repeatedly improving an approximate solution until it is close enough to the true solution. Usually, the longer one iterates, the closer one is able to get to the true solution. The distinctive feature of iterative methods is the rate of convergence, which determines how fast they achieve the solution. To improve the rate of convergence, iterative methods involve a preconditioner that transforms the coefficient matrix into a more favourable spectrum.

The advantage of using iterative methods in solving the EIT problem, is that target accuracies can be chosen that are suitable for each application ranging from low accuracy which only requires quick

calculations up to very accurate solutions that need more iterations for refinement. Figure 2.13 depicts the forward solution using the same mesh and boundary conditions for sequences of tolerance ranging from $1.7x10^{-9}$ to $1.7x10^{-1}$. The conjugate gradient iterative method preconditioned by incomplete Cholesky (ICCG) has been used for solving the forward problem. The figure shows that after seven iterations the error is about 10^{-4}. Performing more iteration does not decrease the boundary error even though the tolerance of the forward solver is getting smaller.

To improve the efficiency of calculating the forward problem in EIT, the tolerance of resistance values can be reduced so that the result matches the measurement accuracy. By recognising that a non-obtuse finite element model can be considered to be equivalent to a resistor network, the accuracy of the resistors in the finite element mesh in section 2.4.3 can be reduced. To study the effect of resistance accuracy in relation to boundary measurements, a finite element mesh with a range of accuracies for the resistor values in the network has been simulated. The boundary voltages resulting from the forward solution are compared to the 'true' data resulting from the fine mesh that is introduced by Gaussian noise. The fine mesh consists of 3,136 elements and 1,633 vertices as mentioned in section 2.4.6.2. In this study 10 different cases of resistance accuracy, 15bits, 14 bits, 13 bits, 12 bits, 11 bits, 10 bits, 9 bits, 8 bits, 7 bits and 6 bits, are compared. To evaluate the various cases, (2.72) is used where V^{fwd} are the predicted voltages resulting from the resistor network with different accuracies. The simulation results are shown in Figure 8.

The graph in Figure 9 shows that the error decreases as the number of bits increases. The error of using 9 bits, 10 bits, 11 bits and 12 bits are 0.08%, 0.03% 0.02% and 0.01%, respectively compared to the 'true' data. On the other hand, the error beyond 12 bits does not go lower than 0.01%. Increasing resistor accuracy in the region 12 bits – 15 bits does not significantly improve the error on the boundary. The results suggest the possibility of constructing a resistor network with low accuracy resistors.

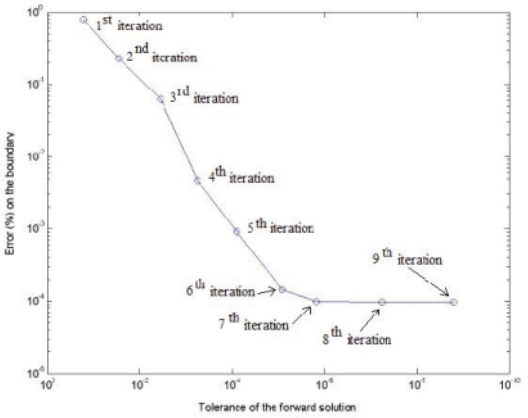

Figure 8: Error of calculated voltages on the boundary

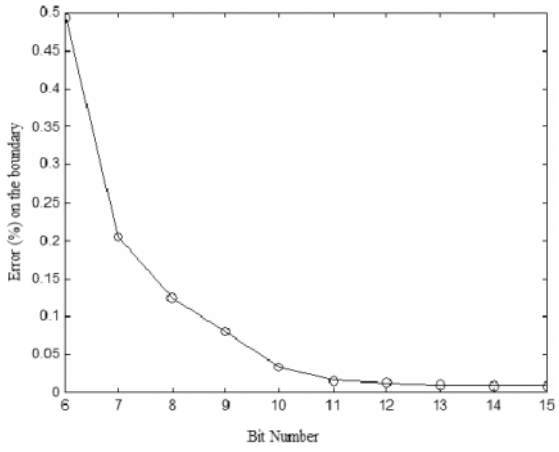

Figure 9: Error of predicted voltages on the boundary of a resistor network

E Conclusion

In this paper, the basic concept of the finite element modelling for electrical resistance tomography has been presented. The complete electrode model, which gives accurate results that agree with physical measurements is incorporated in the forward problem algorithms. FEM, which

is used as a forward problem solver in image reconstructions, transforms the solution of the conductivity equation to a linear system of equations. To solve the linear system of equations in ERT efficiently, the tolerance of the forward solution can be reduced to match the measurement accuracy. The results suggests a 12- bit accuracy can be used.

References

[1] Hinton E., and Owen, D. R. J., "An Introduction to Finite Element Computations", Pineridge Press Limited, Swansea, U.K, 1979.

[2] Zienkiewicz, O. C., (1971), "The Finite Element Method", McGraw-Hill, London, 1971

[3] Carneiro, N. C., and Ramírez-Angulo, J., "High Performance Cell for Solving Real Time Field Problems Using the Resistive Grid Method", IEEE International Conference on Circuits and Systems, May 31 - June 3, Monterrey, CA, 1998.

[4] Nunez, P. L., "Electric field of the brain: the neurophysics of EEG", Oxford University Press, New York, 1981.

[5] Lionheart, W. R. B., "Uniqueness, shape and dimension in EIT", Annals of New York Academy of Sciences, Vol. 873, pp. 466-471, 1999.

[6] Somersalo, E., Cheney, M. and Isaacson, D., "Existence and uniqueness for electrode models for electric current computed tomography", SIAM J Appl Math, Vol. 52, pp. 1023-1040, 1992.

[7] Vauhkonen, M., "Electrical Impedance Tomography and Prior Information", Ph.D Thesis, Kuopio University, Finland, 1997.

[8] Webster, J. G., "Electrical Impedance Tomography", Adam Hilger, 1990.

[9] Melissaratos, E. A., "Optimal Size Finite Element Meshes without Obtuse and Small Angles", Technical Report RUU-CS-92-39, Department of Computer Science Utrecht University, The Netherlands, December, 1992.

[10] Ruppert, J., "A Delaunay Refinement Algorithm for Quality 2-Dimentional Mesh Generation", J. Algorithms, Vol. 18, No. 3, pp. 548-585, May, 1995.

[11] Polydorides, N., "Image Reconstruction Algorithms for Soft-Field Tomography", PhD Thesis, UMIST, 2002.

[12] Komarudin, M., York, T. A., and Lionheart, W. R. B., "Custom silicon for finite element modelling', Proceeding of 2nd World Congress on Industrial Process Tomography, Hannover, Germany, August 2001.

[13] York, T., Komarudin, M., and Lionheart, W. R. B., 'Custom silicon for finite element modelling'. 2nd International Symposium on Process Tomography, Wroclaw, Poland, 2002

[14] Komarudin, M., Lionheart, W. R. B., and York, T. A., "Prototype Hardware for Finite Element Modelling", Proceeding of 3rd World Congress on Industrial Process Tomography, Banff, Canada, 2003.

[15] Komarudin, M., VLSI Implementation of Finite Element Modelling, Dies Natalies Lampung University, Indonesia, August 2006